Improving Parameterization of Entrainment Rate for Shallow Convection with Aircraft Measurements and Large-Eddy Simulation

CHUNSONG LU,[*,+,#,@] YANGANG LIU,[@] GUANG J. ZHANG,[&,**] XIANGHUA WU,[++] SATOSHI ENDO,[@] LE CAO,[##] YUEQING LI,[@@] AND XIAOHAO GUO[*,+]

[*] *Collaborative Innovation Center on Forecast and Evaluation of Meteorological Disasters, Key Laboratory for Aerosol-Cloud-Precipitation of China Meteorological Administration, Nanjing University of Information Science and Technology, Nanjing, China*
[+] *Key Laboratory of Meteorological Disaster of Ministry of Education, Nanjing University of Information Science and Technology, Nanjing, China*
[#] *State Key Laboratory of Numerical Modeling for Atmospheric Sciences and Geophysical Fluid Dynamics, Chinese Academy of Sciences, Beijing, China*
[@] *Biological, Environmental and Climate Sciences Department, Brookhaven National Laboratory, Upton, New York*
[&] *Scripps Institution of Oceanography, University of California, San Diego, La Jolla, California*
[**] *Center for Earth System Science, Tsinghua University, Beijing, China*
[++] *School of Mathematics and Statistics, Nanjing University of Information Science and Technology, Nanjing, China*
[##] *Key Laboratory for Aerosol-Cloud-Precipitation of China Meteorological Administration, Nanjing University of Information Science and Technology, Nanjing, China*
[@@] *Institute of Plateau Meteorology, China Meteorological Administration, Chengdu, China*

(Manuscript received 19 February 2015, in final form 28 September 2015)

ABSTRACT

This work examines the relationships of entrainment rate to vertical velocity, buoyancy, and turbulent dissipation rate by applying stepwise principal component regression to observational data from shallow cumulus clouds collected during the Routine Atmospheric Radiation Measurement (ARM) Aerial Facility (AAF) Clouds with Low Optical Water Depths (CLOWD) Optical Radiative Observations (RACORO) field campaign over the ARM Southern Great Plains (SGP) site near Lamont, Oklahoma. The cumulus clouds during the RACORO campaign simulated using a large-eddy simulation (LES) model are also examined with the same approach. The analysis shows that a combination of multiple variables can better represent entrainment rate in both the observations and LES than any single-variable fitting. Three commonly used parameterizations are also tested on the individual cloud scale. A new parameterization is thus presented that relates entrainment rate to vertical velocity, buoyancy, and dissipation rate; the effects of treating clouds as ensembles and humid shells surrounding cumulus clouds on the new parameterization are discussed. Physical mechanisms underlying the relationships of entrainment rate to vertical velocity, buoyancy, and dissipation rate are also explored.

1. Introduction

Cumulus clouds play key roles in climate and weather through the transport of moisture, heat, and momentum (Arakawa and Schubert 1974). Representation of cumulus convection in large-scale models significantly affects the simulations of precipitation (Del Genio and Wu 2010; Wang et al. 2007, 2011), Madden–Julian oscillation (Cai et al. 2013; Zhang and Song 2009), and El Niño–Southern Oscillation (Wu et al. 2007).

A fundamental quantity in convection parameterizations is fractional entrainment rate λ, which is defined as the fractional air mass entrained into a volume of cloudy air per unit height (Betts 1975; Blyth 1993; Romps 2010). A variety of expressions have been proposed to parameterize λ over the last few decades. For example, Turner (1962) and Squires and Turner (1962) proposed that λ is inversely proportional to cloud radius. Lin (1999) presented an expression relating λ to buoyancy B: $\lambda \propto B^{\phi}$, where ϕ is an empirical parameter. Von Salzen and McFarlane (2002) related λ to vertical gradient of buoyancy: $\lambda \propto dB/dz$. Dawe and Austin (2013)

Corresponding author address: Chunsong Lu, NUIST, Room 1010, Qixiang Bldg., No. 219, Ningliu Road, Nanjing, Jiangsu 210044, China.
E-mail: luchunsong110@hotmail.com

DOI: 10.1175/JAS-D-15-0050.1

found that λ could be fitted by $\lambda \propto (Bd\overline{\theta}_\rho/dz)^\gamma$, where $\overline{\theta}_\rho$ is the density potential temperature (the bar denotes the horizontal mean over the entire model domain) and γ is an empirical parameter. Neggers et al. (2002) proposed that λ is inversely proportional to vertical velocity w. Gregory (2001) related λ to B/w^2. Grant and Brown (1999) proposed that λ is proportional to the fraction of turbulent kinetic energy production that is available for entrainment. Some studies attempted to relate entrainment rate to B/w^2 and $w^{-1}dw/dz$ (e.g., de Rooy and Siebesma 2010; Wang and Zhang 2014).

Most existing parameterizations have been developed based on numerical simulations, and observationally based studies are much needed to evaluate them. The primary objectives of this study are threefold: 1) to examine the relationships of λ to the variables commonly used in existing parameterizations by analyzing the data on shallow cumulus clouds collected during the Routine Atmospheric Radiation Measurement (ARM) Aerial Facility (AAF) Clouds with Low Optical Water Depths (CLOWD) Optical Radiative Observations (RACORO) field campaign over the ARM Southern Great Plains (SGP) site near Lamont, Oklahoma, from 22 January to 30 June 2009 (Schmid et al. 2014; Vogelmann et al. 2012), 2) to develop a new parameterization of entrainment rate, and 3) to evaluate the new and existing parameterizations by comparing with one another and with that calculated from the observations. The RACORO cumulus clouds simulated with a large-eddy simulation (LES) model (Endo et al. 2015; Lin et al. 2015) are also analyzed with the same approach and compared against the observational results.

2. Observational data

During RACORO, comprehensive measurements of cloud, aerosol, radiation, and atmospheric state variables were made by the instrumented Twin Otter aircraft from the Center for Interdisciplinary Remotely-Piloted Aircraft Studies (CIRPAS). Temperature, water vapor, and w were measured with a Rosemount probe, diode laser hygrometer (DLH) (Diskin et al. 2002; Podolske et al. 2003), and a five-hole gust probe, respectively. Turbulent dissipation rate ε is calculated using the method developed by Chan et al. (1998). The cloud and aerosol spectrometer (CAS) was used to measure cloud droplet spectra at 10 Hz, which are used to calculate liquid water content (LWC).

Eight shallow cumulus flights (22, 23, and 24 May and 11, 19, 23, 24, and 26 June 2009) are analyzed based on the conditional sampling of actively growing clouds. The criteria are as follows: 1) Cloud droplet size distributions must have LWC $> 0.001\ \mathrm{g\,m^{-3}}$ and cloud droplet number concentration greater than $10\ \mathrm{cm^{-3}}$ (e.g., Deng et al. 2009; Lu et al. 2012a). Two neighboring cloud droplet size distribution samples must be less than 50 m apart in order for them to be considered within the same cloud. 2) The percentage of data points with positive vertical velocity within an individual cloud is larger than 80% (Gerber et al. 2008; Lu et al. 2012c). 3) An individual cloud must have more than 30 cloud droplet size distributions (the data were collected at approximately 5-m spatial resolution with the CAS sampling rate of 10 Hz and an aircraft speed of about $50\ \mathrm{m\,s^{-1}}$). 4) An individual cloud must be farther than 1500 m from other clouds (Lu et al. 2014b). 5) The mean buoyancy B in an individual cloud must be larger than $0.005\ \mathrm{m\,s^{-2}}$; B is calculated using the equation

$$B = \frac{T_{vc} - T_{ve}}{T_{ve}} g, \tag{1}$$

where T_{vc} and T_{ve} are virtual temperature in cloud and environment, respectively; g is the gravity acceleration. Virtual temperature T_v is defined as

$$T_v = T(1 + 0.608q), \tag{2}$$

where T is temperature and q is water vapor mixing ratio. The empirical equation based on Fig. 8b in Lawson and Cooper (1990) is used to correct temperature for the wet cooling:

$$T = T_m + \alpha \mathrm{LWC}, \tag{3}$$

where T_m is the temperature measured by the Rosemount probe; T is the corrected temperature; we use 0.5 for α. Note that the aircraft speed is about $50\ \mathrm{m\,s^{-1}}$ in this study, only half of that ($\sim 100\ \mathrm{m\,s^{-1}}$) in Lawson and Cooper (1990), so the temperature is expected to be less sensitive to LWC, and α used for this study might be smaller than 0.5. To be conservative, the above-mentioned sampling condition of mean $B > 0.005\ \mathrm{m\,s^{-2}}$ must be satisfied with both corrected ($\alpha = 0.5$) and uncorrected ($\alpha = 0$) temperature. A total of 102 actively growing cumulus clouds (16.9% of all the cloudy point data) satisfy these criteria described above. Cumulus cloud depths in RACORO are typically about 200–500 m (Vogelmann et al. 2012). The cloud core widths in the 102 clouds have a wide range of values, with the mean and standard deviation being 431 and 275 m, respectively, where the edge of a cloud core is defined as the point along the direction from the cloud edge toward the cloud interior where downdraft changes to updraft for the first time [see Fig. 1 in Lu et al. (2012b) for details].

Entrainment rate is calculated for each cloud penetration using the mixing fraction approach of Lu et al. (2012c). See Lu et al. (2012b, 2013) for more details on

the calculation of λ. The mean temperature and water vapor mixing ratio in the air with a distance from D to $2D$ from the edge of a cloud core are taken to be the properties of the dry air entrained into the clouds (Lu et al. 2012b). Here, D is set to be 500 m. The reason for using this value is that the mean state of the dry air with $D = 500$ m is close to that from the aircraft vertical sounding, which could represent the environmental air far away from clouds; the entrainment rate calculated with $D = 500$ m is recommended for the widely used cumulus parameterization scheme including only cloud and environment (Lu et al. 2012b, 2014a).

In the above criteria for filtering clouds, several arbitrary thresholds are used. Lu et al. (2012b) studied the sensitivity of λ to these thresholds by increasing or decreasing the thresholds by 50% and found that the relative difference of entrainment rate was in the range of 3%–8%.

3. Large-eddy simulation

The cumulus clouds occurring on 22, 23 and 24 May 2009 were simulated using the Advanced Research version of the Weather Research and Forecasting (WRF) Model (ARW), implemented with forcing ingestion and other functions to constitute a flexible LES in the Fast-Physics System Test Bed and Research (FASTER) project (WRF-FASTER) (Endo et al. 2015). For these simulations, WRF-FASTER uses a fully compressible equation system with a prognostic turbulent kinetic energy scheme (Deardorff 1980), a two-moment microphysics scheme (Morrison et al. 2005), and Rapid Radiative Transfer Model (RRTM) scheme (Mlawer et al. 1997) adopted from the Cloud Feedbacks Model Intercomparison Project (CFMIP)/Global Atmospheric System Studies (GASS) Intercomparison of Large-Eddy and Single-Column Models (CGILS) project (Blossey et al. 2013). The model input includes the time-varying quad-modal aerosol size distribution profiles and hygroscopicity parameters developed in Vogelmann et al. (2015) and the Atmospheric Radiation Measurement Constrained Variational Analysis (VARANAL) forcing product (Xie et al. 2004; Zhang et al. 2001). The simulation has a domain size of $9.6 \times 9.6\,\mathrm{km}^2$, 128×128 horizontal grid points with a 75-m resolution, and a vertical resolution of approximately 40 m for the 125 levels below 5 km and a sponge layer for 13 grid levels up to 5.5 km. The simulation time is from 0600 local time (LT; UTC minus 6 h) 22 May through 1800 LT 24 May.

As shown in Fig. 6 of Endo et al. (2015), the 3-day cumulus evolution was successfully simulated. The following sampling is used to mimic the aircraft observations during RACORO. If i is used to denote the 128 grid points in the west–east direction, an aircraft is assumed to collect the data in south–north direction at $i = 16, 32, 48, 64, 80, 96, 112$ at the vertical level of 50 (~2000-m height) for each 10-min-interval output. The reason for choosing level 50 is that this level can be near cloud base, in the middle of cloud, or near cloud top at different times because of the variations of cloud bases and tops with time. Similar to treating observations, effective cloud samples must have liquid water mixing ratio larger than $0.001\,\mathrm{g\,kg^{-1}}$ (close to $0.001\,\mathrm{g\,m^{-3}}$ used for sampling the observational data) and cloud droplet number concentration larger than $10^7\,\mathrm{kg^{-1}}$ (close to $10\,\mathrm{cm^{-3}}$). Cloud sizes must be larger than 150 m, equivalent to 30 cloud droplet size distributions in the aircraft observations. Mean buoyancy in a cloud must be larger than $0.005\,\mathrm{m\,s^{-2}}$, and 80% of the data points in a cloud must have positive vertical velocity. In total, there are 215 actively growing cloud samples satisfying these criteria. To calculate entrainment rate, the dry air entrained into clouds is assumed to have the mean properties (e.g., temperature and relative humidity) of the environmental air at the level of 50.

4. Results

a. *Relationships between entrainment rate, vertical velocity, dissipation rate, and buoyancy*

This section examines the measurements for the relationships of λ to the dynamical/thermodynamic quantities commonly used in previous studies of entrainment rate parameterizations: w, B, ε, and B/w^2 (Fig. 1). It is evident that λ is negatively correlated with w, B, and ε but positively correlated with B/w^2 for both the observed and simulated clouds. All these individual pairs can be fitted with a power-law function

$$\lambda = ax^b, \tag{4}$$

where x represents w, B, ε or B/w^2; a and b are two empirical parameters. The negative correlation between λ and w from both the observations and the LES supports the results of previous studies (Dawe and Austin 2013; Neggers et al. 2002). Lin (1999) and Dawe and Austin (2013) also found a negative correlation between λ and B based on numerical simulations. The positive correlation between λ and B/w^2 is consistent with the theoretical analysis by Gregory (2001) and de Rooy and Siebesma (2010).

The adjusted coefficient of determination R^2 is used to measure the goodness of the fit to the data and will be used to compare the results in Fig. 1 with the results from principal component regression shown later. It

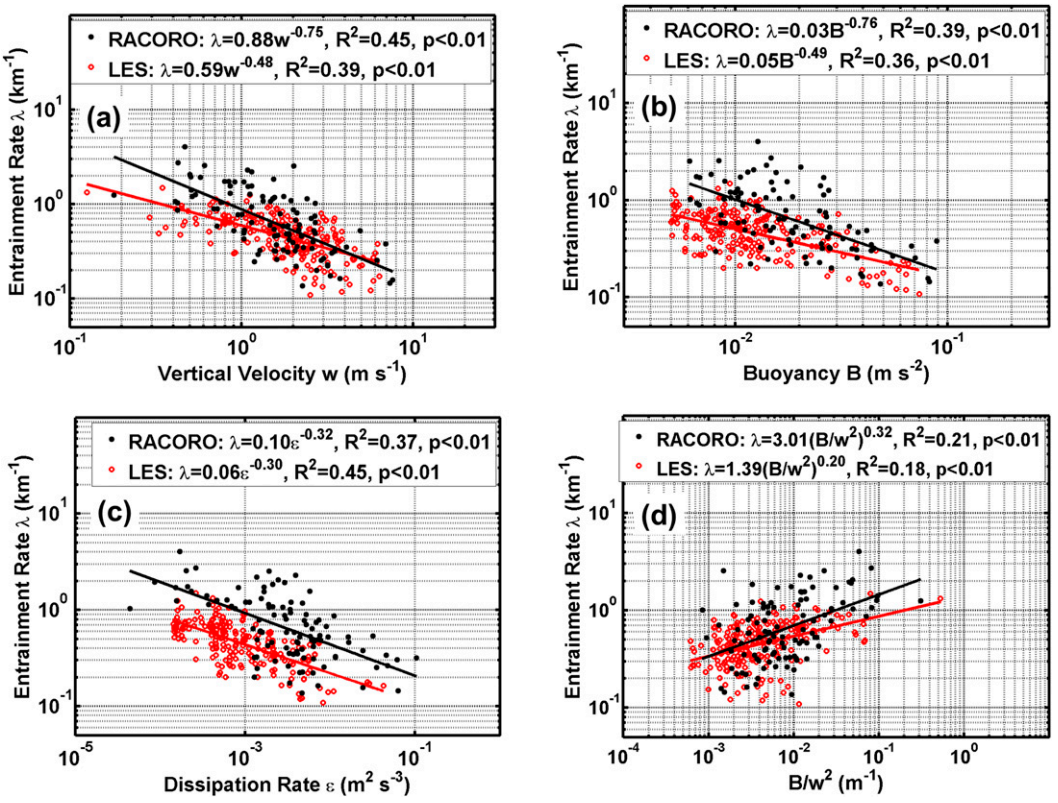

FIG. 1. Relationships between entrainment rate λ and (a) vertical velocity w, (b) buoyancy B, (c) dissipation rate ε, and (d) B/w^2 in 102 actively growing cumulus clouds during RACORO. Also shown for comparison are the results from 215 actively growing cumulus clouds sampled from the LES. The parameter R^2 is the adjusted coefficient of determination and p shows the significance level.

represents the fraction of the variance in entrainment rate explained by the dependent variable. The λ is related to all the variables with the adjusted $R^2 = 0.45$, 0.39, 0.37, and 0.21 for the correlations between λ and w, B, ε, and B/w^2, respectively, in the observed clouds. Similar results are found for simulated clouds, with the corresponding values of R^2 being 0.39, 0.36, 0.45, and 0.18, respectively. Note that all the correlations are statistically significant with the p values smaller than 0.01. Here, only one dependent variable is used in the regression; the fitting parameters a and b will change when more variables are included in the fitting equation, as will be examined in section 4b.

The negatively correlated relationships of λ with w, B, and ε are related to the interactions among the quantity-related processes. It is physically consistent that a larger λ leads to smaller B, w, and ε. The temperature of the environmental air entrained into the clouds is lower than that in the clouds, and evaporation of droplets during mixing processes between dry air and cloudy air also decreases the temperature in the clouds. As a result, B is smaller when λ is larger. A smaller B in turn leads to smaller w and ε because B is the primary driver of w and ε. In addition, turbulence near the cloud edge associated with entrainment also creates form drag that acts to decelerate w. A smaller in-cloud w means a smaller horizontal shear of w in and outside clouds, leading to weaker turbulence (i.e., a smaller ε) in clouds. The interactions among B, w, and ε are responsible for the positive correlations among the three variables (Fig. 2). Furthermore, a cloud with smaller w takes more time to rise to a certain height and has more time to interact with the environment, thus leading to a larger λ (Neggers et al. 2002); we note that λ represents fractional entrainment of air mass per unit distance. The negative correlation between λ and w and the positive correlations among ε, B, and w are responsible for the negative correlations between λ and B and ε. The mutual correlations between λ, B, and w are also responsible for the positive correlation between λ and B/w^2.

b. A new parameterization for entrainment rate

The scatter of data points in Fig. 1 suggests that λ should be better parameterized as a joint function of all the variables examined (i.e., w, B, ε, and B/w^2)

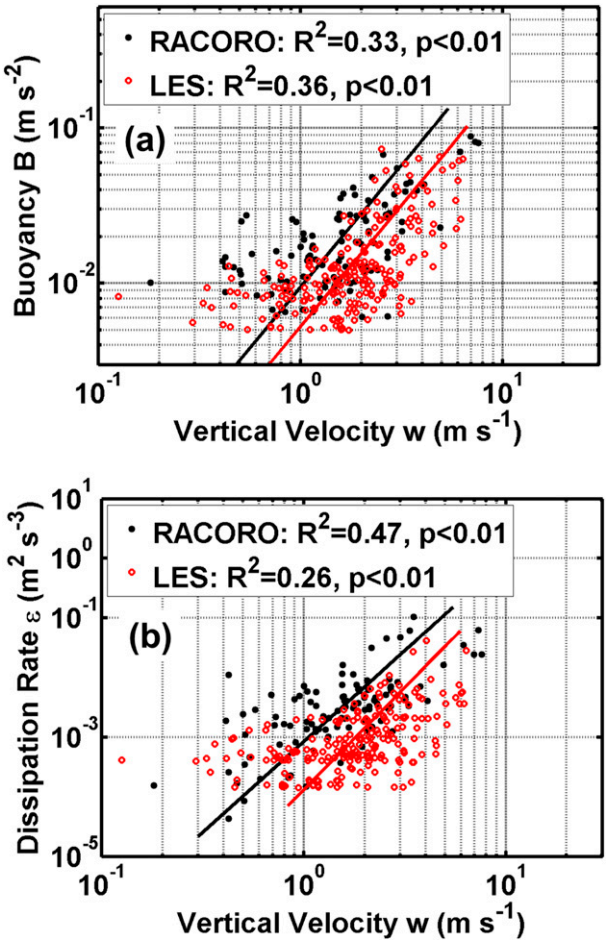

FIG. 2. Relationships between (a) buoyancy B and vertical velocity w and (b) dissipation rate ε and w in 102 actively growing cumulus clouds observed during RACORO and 215 actively growing cumulus clouds sampled from the LES. The parameter R^2 is the adjusted coefficient of determination and p shows the significance level.

instead of an individual variable alone as done in most previous studies. To explore the multivariate aspect and develop a new parameterization, multivariable regressions are performed by adding one independent variable at a time. For multivariable regressions, the adjusted R^2 increases only if the newly added variable improves the fitting model more than would be expected by chance (Bajpai 2009). In view of the significant partial correlations between all the variables for both the observed and simulated clouds (Fig. 2), the approach of principal component regression is used to minimize the mutual dependence among the properties (Jolliffe 1982). In statistics, principal component regression is a regression analysis technique based on principal component analysis. Take logarithms of λ, w, B, and ε and apply principal component regression; the fitting equations in the exponent forms, together with the adjusted R^2 and the p values, are summarized below:

$$\lambda = 0.11 w^{-0.45} B^{-0.50} \quad (\text{Adjusted } R^2 = 0.51;\ p < 0.01) \tag{5a}$$

and

$$\lambda = 0.072 w^{-0.31} B^{-0.36} \varepsilon^{-0.15} \quad (\text{Adjusted } R^2 = 0.53;\ p < 0.01) \tag{5b}$$

for the observed clouds, and

$$\lambda = 0.13 w^{-0.29} B^{-0.31} \quad (\text{Adjusted } R^2 = 0.50;\ p < 0.01) \tag{6a}$$

and

$$\lambda = 0.056 w^{-0.18} B^{-0.24} \varepsilon^{-0.16} \quad (\text{Adjusted } R^2 = 0.57;\ p < 0.01) \tag{6b}$$

for the simulated clouds. In the observed clouds, Eq. (5) shows a gradual increase of the adjusted R^2 when more independent variables are added in the regression, while the values of adjusted R^2 for individual regressions shown in Fig. 1 are in the range 0.21–0.45. Similar conclusions can be reached for the simulated clouds. This gradual increase of the adjusted R^2 with more independent variables suggests that considering all the variables improves representation of entrainment rate.

c. *Examination of the new and existing parameterizations*

In view of their widespread use, this section examines the new parameterization and some existing parameterizations by comparing against observations/simulations. One of the existing parameterizations to be evaluated is that proposed by Neggers et al. (2002):

$$\lambda = \frac{\eta}{\tau}\frac{1}{w}, \tag{7}$$

where τ is the eddy turnover time scale and is approximately 300 s for shallow cumulus clouds; η is an empirical parameter. The other is that proposed by Gregory (2001) whereby λ is represented by B/w^2 instead of w:

$$\lambda = C_\lambda a B/w^2 = CB/w^2, \tag{8}$$

where $a = 1/6$, $C_\lambda = 1/2$, and $C = 1/6 \times 1/2 = 0.08$ for shallow cumulus clouds. Neggers et al. (2002) applied their parameterization to individual convective parcels. The multiparcel parameterization was used to give the

right vertical profile of domain-mean mass flux, thermodynamic properties of the ensemble, etc. Gregory's (2001) parameterization works for ensemble-mean λ, B, and w. So both of their targets are parameterizations for ensemble-mean properties. Here we apply them to individual clouds to test if and how they work on the individual cloud scale. In practice, the empirical parameters η and C are taken to be constants; thus, we first evaluate this assumption by applying the observational and numerical results in the individual clouds to the equations $\eta = \lambda\tau w$ and $C = \lambda w^2/B$ for the Neggers et al. and Gregory et al. schemes, respectively. A similar approach was used by Del Genio and Wu (2010) to check if η or C is a constant using domain-mean properties. Figure 3a shows that, instead of being a constant, η exhibits a wide range of variation from 0.068 to 1.54 for the observed clouds and a range from 0.048 to 0.74 for the simulated clouds. Del Genio and Wu (2010) also found that η had significant variations for domain-mean properties. Likewise, Fig. 3b shows that the values of C range from 0.004 to 1.7 for the observed clouds and from 0.0025 to 0.79 for the simulated clouds. In addition, Lin (1999) related entrainment rate to B with Eq. (4). The exponent b in this study is -0.76 for the observed clouds and -0.49 for the simulated clouds (Fig. 1b), larger than -1.12, -1.09, -1.25, and -1.48 in Lin (1999); the reason could be that b may be related to large-scale environments, as pointed out by Lin (1999). Also, Lin (1999) used ensemble properties; instead, the properties on the individual cloud scale are used here. These results reinforce the conclusion that more independent variables should be used to parameterize λ.

Figures 4 and 5 compare λ derived from the new and previous parameterizations with the values calculated using the mixing fraction approach. In Fig. 4a, η is taken to be 0.15 and 0.35 for the observed clouds, because 0.15 is the middle value of the peak bin and 0.35 is the mean η in the clouds. Similarly, η is taken to be 0.15 and 0.27 for the simulated clouds (Fig. 4c). The result with η equal to 0.15 significantly underestimates entrainment rate for both the observed and simulated clouds. Although the data points with η equal to 0.35 (Fig. 4a) or 0.27 (Fig. 4c) distribute almost evenly along the one-to-one line, they are scattered. In Fig. 4b, C is taken to be 0.06 and 0.14 for the observed clouds because 0.06 is the middle value of the peak bin and 0.14 is the mean C in the clouds. Similarly, C is taken to be 0.06 and 0.16 for the simulated clouds (Fig. 4d). No matter which C is taken, the results are quite scattered for both the observed and simulated clouds. When η or C is taken to be a constant, the fitting equations in the simulated clouds have larger adjusted R^2 than those in the observed clouds. For example, when $\eta = 0.15$, the adjusted

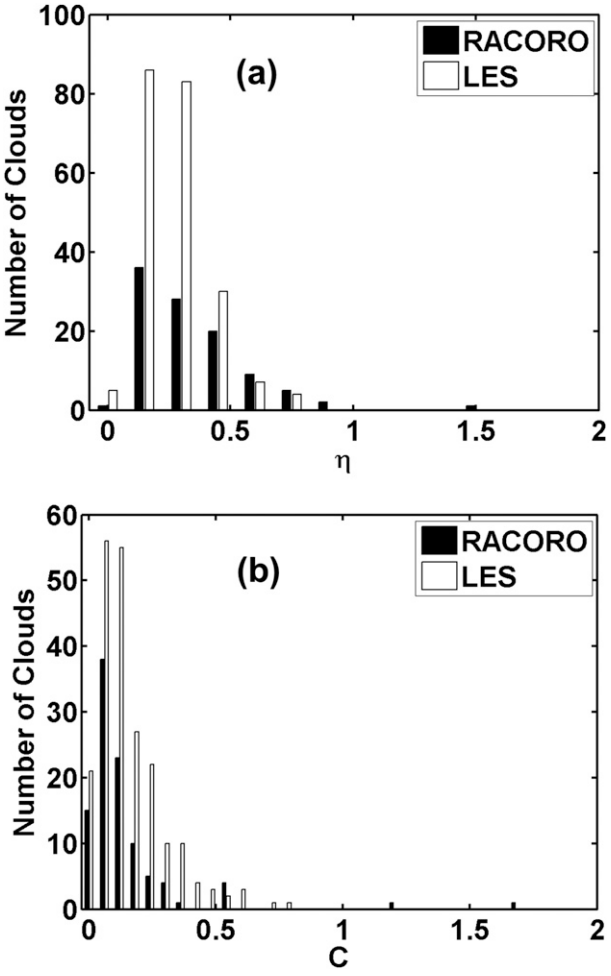

FIG. 3. Histograms of (a) η in Neggers et al.'s (2002) parameterization and (b) C in Gregory's (2001) parameterization, derived from 102 actively growing cumulus clouds observed during RACORO and 215 actively growing cumulus clouds sampled from the LES.

R^2 in Eq. (7) for the simulated clouds is 0.30, whereas the adjusted R^2 for the simulated clouds is 0.25 (Figs. 4a and 4c). The reason is that the distributions of η and C have sharper peaks in the simulated clouds than in the observed clouds.

For the single-variable fittings, λ and w have the largest adjusted R^2 in the observed clouds, whereas λ and ε have the largest adjusted R^2 in the simulated clouds (Figs. 4 and 5). Using all three variables (w, B, ε) makes the fitting better than using two or one variable. The data points for the fitting equations in Fig. 5 generally fall along the one-to-one line, but all the fitting equations tend to underestimate entrainment rate when it is large, with the least overestimation by Eqs. (5b) and (6b), which consider the most independent variables, including ε (Fig. 5d). Although ε can improve the fitting with the adjusted R^2 increased from 0.51 to 0.53 in the

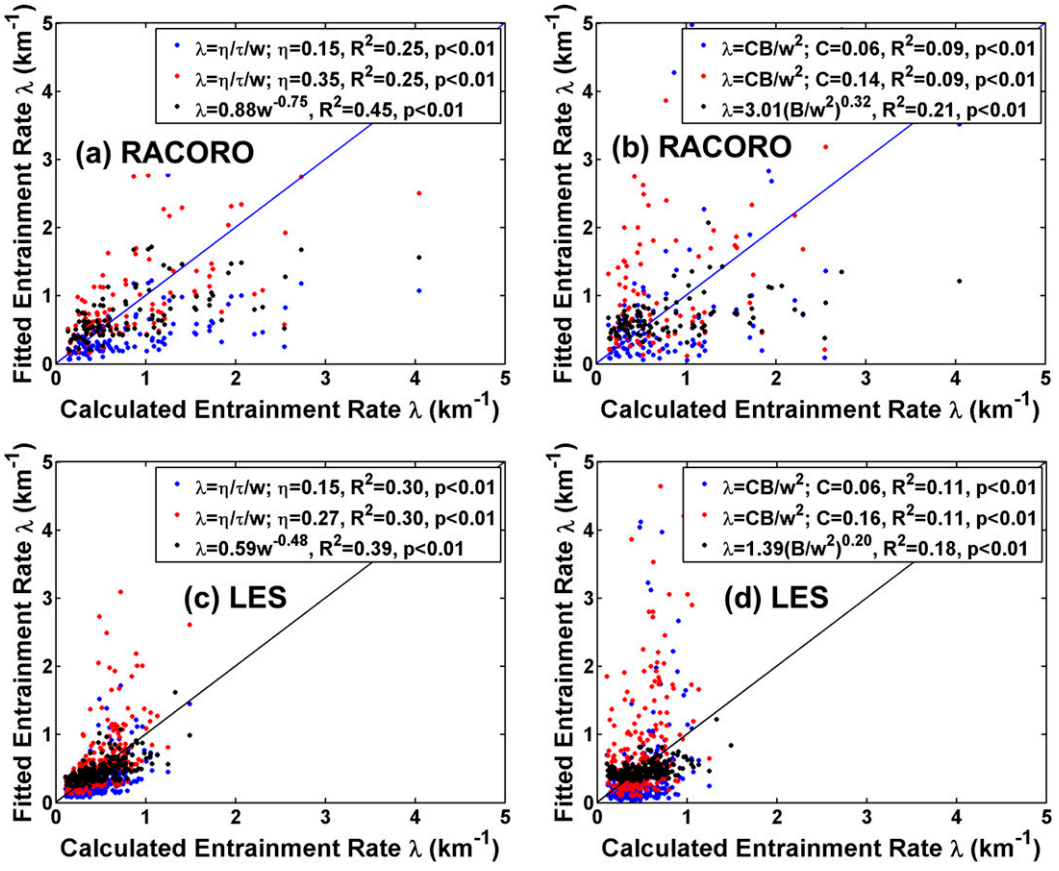

FIG. 4. Fitted entrainment rate as a function of calculated entrainment rate in 102 actively growing cumulus clouds observed during RACORO and 215 actively growing cumulus clouds sampled from the LES. Fitted entrainment rate is calculated using the fitting equations from (a),(c) vertical velocity w and (b),(d) B/w^2, where B is buoyancy. The x-axis label is the entrainment rate calculated using the mixing-fraction approach. The parameter R^2 is the adjusted coefficient of determination and p shows the significance level. The R^2 values for blue and red dots are the same because logarithms are taken in calculating R^2, to be consistent with the R^2 calculations for black dots.

observed clouds and from 0.50 to 0.57 in the simulated clouds, since it is not available in large-scale models for existing cumulus parameterizations, the equations with only B and w are more appropriate for present use (Fig. 5c).

It should be pointed out that although the best fit does reasonably well in matching the retrieved entrainment rate, it is unknown whether it gives useful profiles of cloud fraction and mass flux, or whether the fit would be the same in a very different shallow cumulus environment, such as over the subtropical oceans.

5. Further discussions

The comparison shows that the observed and simulated clouds (Figs. 1, 4, and 5) exhibit similar relationships among λ, w, B, and ε, using the similar sampling method. This result supports the approach and thus obtained entrainment rate parameterizations even for observations with potential measurement errors. The results also suggest that WRF-FASTER as an LES model can reproduce the key entrainment-related quantities and their relationships reasonably well. Qualitatively, the cloud-mean B, w, ε, and λ from the LES have similar ranges to those in the observed clouds (Fig. 1). Quantitatively, the mean and standard deviation values from the LES from 22 to 24 May 2009—that is, w ($2.1 \pm 1.3\,\mathrm{m\,s^{-1}}$), B ($0.016 \pm 0.013\,\mathrm{m\,s^{-2}}$), ε ($0.0019 \pm 0.0042\,\mathrm{m^2\,s^{-3}}$), and λ ($0.51 \pm 0.24\,\mathrm{km^{-1}}$)—are comparable with the observations on the 8 days—that is, w ($1.9 \pm 1.4\,\mathrm{m\,s^{-1}}$), B ($0.022 \pm 0.017\,\mathrm{m\,s^{-2}}$), ε ($0.0077 \pm 0.015\,\mathrm{m^2\,s^{-3}}$), and λ ($0.86 \pm 0.69\,\mathrm{km^{-1}}$), respectively. In addition, the quantities in the observed clouds from 22 to 24 May 2009 are w ($2.1 \pm 1.4\,\mathrm{m\,s^{-1}}$), B ($0.020 \pm 0.020\,\mathrm{m\,s^{-2}}$), ε ($0.011 \pm 0.020\,\mathrm{m^2\,s^{-3}}$), and λ ($0.80 \pm 0.55\,\mathrm{km^{-1}}$). If only focused on the observed and simulated clouds from 22 to 24 May 2009, the mean and standard deviation values of w, B, and λ, except ε,

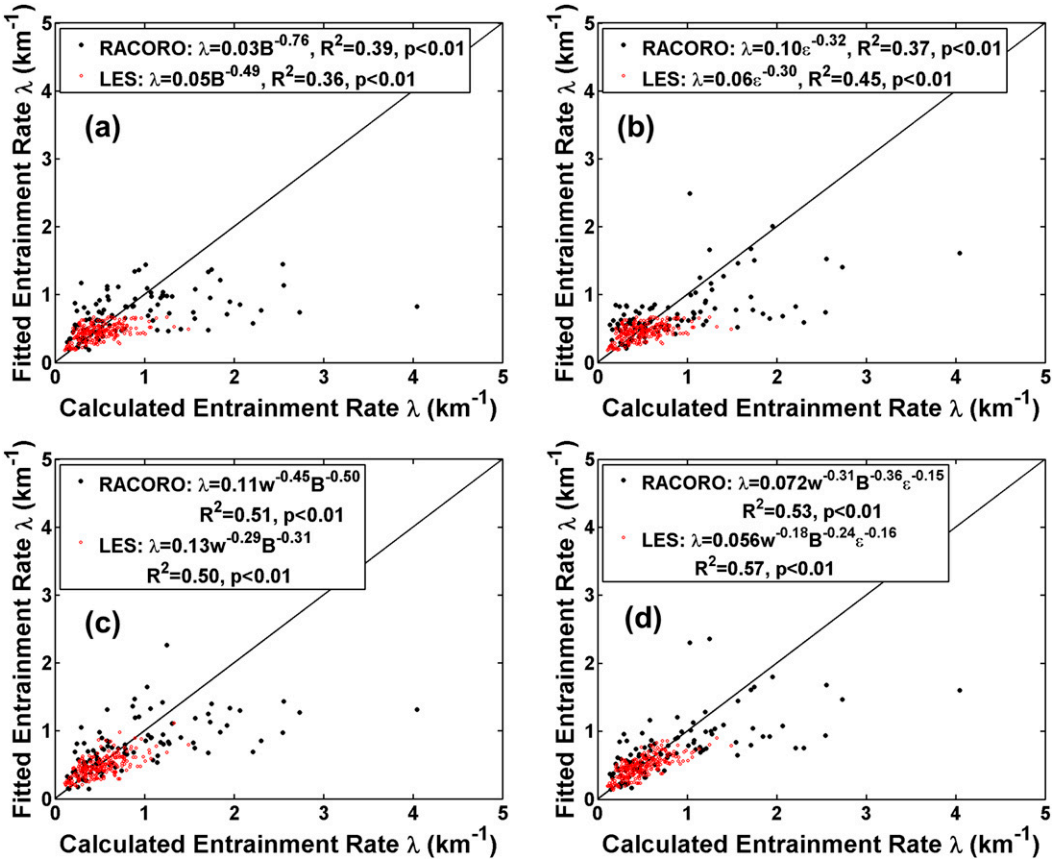

FIG. 5. Relationship between fitted entrainment rate and calculated entrainment rate in 102 actively growing cumulus clouds observed during RACORO and 215 actively growing cumulus clouds sampled from the LES. Fitted entrainment rate is calculated using the fitting equations from (a) buoyancy B, (b) turbulent dissipation rate ε, (c) w and B, and (d) w, B, and ε. The x-axis label is the entrainment rate calculated using the mixing fraction approach. The parameter R^2 is the adjusted coefficient of determination and p shows the significance level.

are even closer. In addition, the relationship between λ and ε has the largest adjusted R^2 for the simulated clouds. Furthermore, the relationships between λ and ε in the observed and simulated clouds have a similar slope (Fig. 1c); the exponent b in Eq. (4) is -0.32 for the observed clouds, close to -0.30 for the simulated clouds. Thus, the LES model may underestimate ε but still well captures the variation trends of ε in different clouds.

Parameterizations of entrainment rate in large-scale models are for the collective effect of cloud ensembles within a model grid. It is thus interesting to examine the difference of the results between the individual clouds and cloud ensembles. As explained before, the 215 individual cloud samples are collected at the level of 50 (2000-m height) in 86 snapshots of the LES. For each snapshot, cloud properties (e.g., LWC, temperature, water vapor mixing ratio, w, B, and ε) in the selected clouds are calculated as the cloud-ensemble properties; then λ for the cloud ensemble is calculated using the cloud-ensemble properties. Based on the 86 samples of cloud ensembles, the relationships of λ with w, B, ε, and B/w^2, and the mutual relationships among w, B, and ε (not shown) are similar to the results for individual clouds shown in Figs. 1 and 2. The fitting equations with two and three properties are

$$\lambda = 0.17 w^{-0.31} B^{-0.27} \quad (\text{Adjusted } R^2 = 0.38;\ p < 0.01) \tag{9a}$$

and

$$\lambda = 0.089 w^{-0.18} B^{-0.15} \varepsilon^{-0.16} \quad (\text{Adjusted } R^2 = 0.45;\ p < 0.01). \tag{9b}$$

Equations (9a) and (9b) are similar to Eqs. (6a) and (6b), respectively, though the coefficients and adjusted R^2 are different because of the ensemble effect. Figure 6 also shows that the results from the 215 individual cloud samples and the 86 cloud ensembles are similar. Generally, the data points fall along the one-to-one line, and

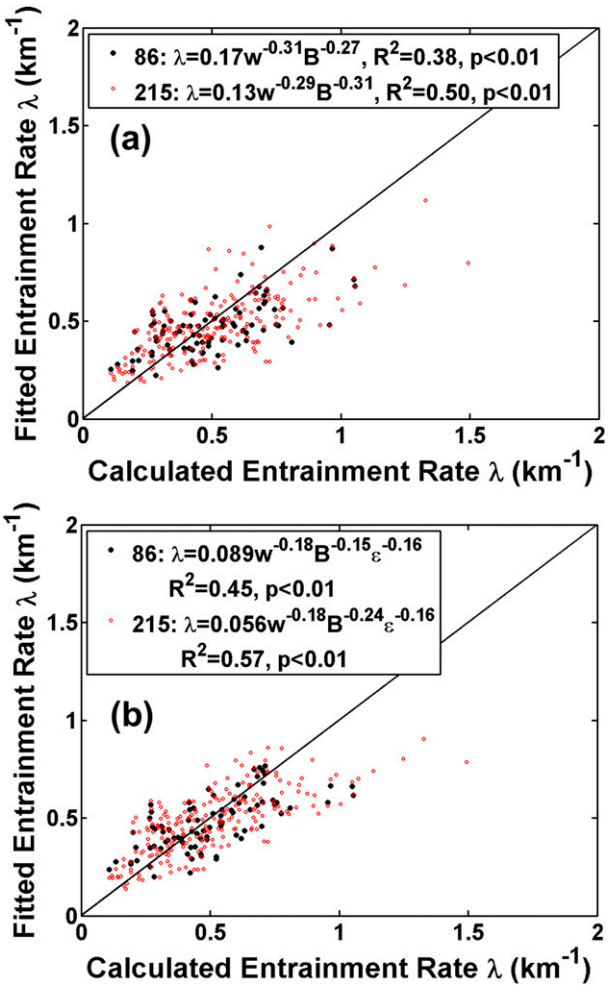

FIG. 6. Relationship between fitted entrainment rate and calculated entrainment rate in 215 actively growing cumulus cloud samples and 86 cloud ensembles in the LES. Fitted entrainment rate is calculated using the fitting equations from (a) vertical velocity w and buoyancy B and (b) w, B, and dissipation rate ε. The x axis is the entrainment rate calculated using the mixing fraction approach. The parameter R^2 is the adjusted coefficient of determination and p shows the significance level.

the three-variable fitting has a smaller scatter than the two-variable fitting for both individual cloud samples and cloud ensembles.

Another interesting topic is the effect of different sources of dry air on the calculated entrainment rates (Lu et al. 2012b) and the fitting equations. As shown in Fig. 3 of Lu et al. (2012b), temperature in the assumed entrained air is lower and relative humidity is higher with $D = 10$ m than with $D = 500$ m because the assumed entrained air is mainly from the humid shells surrounding cumulus clouds (Heus and Jonker 2008) with $D = 10$ m. The fitting equations for $D = 10$ m based on the principal component regression are

$$\lambda = 0.16w^{-0.55}B^{-0.68} \quad (\text{Adjusted } R^2 = 0.60;\ p < 0.01) \tag{10a}$$

and

$$\lambda = 0.069w^{-0.36}B^{-0.67}\varepsilon^{-0.14} \quad (\text{Adjusted } R^2 = 0.63;\ p < 0.01). \tag{10b}$$

The relationships of λ with w, B, and ε are still valid after considering the effects of the humid shells in terms of the coefficient signs, adjusted R^2, and p; the R^2 values are even higher than for $D = 500$ m.

The Buckingham–Pi analysis provides an alternative to finding the relationships of entrainment rate to related variables. Since cloud radius r (Simpson 1971) and vertical divergence $(1/w)(dw/dz)$ (de Rooy and Siebesma 2010) were used in previous studies on entrainment rate, the two properties are also included when applying the Buckingham–Pi theorem, besides w, B, and ε. The Buckingham–Pi theorem states that if there is a physically meaningful equation involving n physical variables, then the original equation can be rewritten in terms of a set of $n - k$ dimensionless parameters constructed from the original variables. Here k is the number of physical dimensions involved. In our case, two dimensions, L and t, are included, which means $k = 2$. Therefore, two variables, B and w, which cover both of the two dimensions are used to nondimensionalize other quantities:

$$\begin{aligned}\lambda &= \sum_i a_i B^{b_{1i}+b_{2i}+b_{3i}} w^{c_{1i}+c_{2i}+c_{3i}} \varepsilon^{d_i} \left(\frac{1}{r}\right)^{e_i} \left(\frac{1}{w}\frac{dw}{dz}\right)^{f_i} \\ &= \sum_i a_i [B^{b_{1i}} w^{c_{1i}} \varepsilon^{d_i}] \left[B^{b_{2i}} w^{c_{2i}} \left(\frac{1}{r}\right)^{e_i}\right] \left[B^{b_{3i}} w^{c_{3i}} \left(\frac{1}{w}\frac{dw}{dz}\right)^{f_i}\right],\end{aligned} \tag{11}$$

where a_i is a parameter and b_{1i}, b_{2i}, b_{3i}, c_{1i}, c_{2i}, c_{3i}, d_i, e_i, and f_i are exponents, which are often taken to be integers, such as -1, 0, and 1. Therefore, λ can be written as the sum of i terms including w, B, ε, r, and $(1/w)(dw/dz)$, where $i = 1, 2, 3, \ldots$, and the maximum i depends on the power of Eq. (11) according to the requirement of accuracy. To keep the units at the left- and right-hand sides of Eq. (11) equal, one of the three quantities—$B^{b_{1i}} w^{c_{1i}} \varepsilon^{d_i}$, $B^{b_{2i}} w^{c_{2i}} (1/r)^{e_i}$, and $B^{b_{3i}} w^{c_{3i}} [(1/w)(dw/dz)]^{f_i}$—must have the same unit as λ and the rest have the unit of one. Regardless of the specific choice, all lead to the same result:

$$\frac{\lambda}{B/w^2} = \sum_i a_i \left(\frac{\varepsilon}{Bw}\right)^{d_i} \left(\frac{w^2}{Br}\right)^{e_i} \left(\frac{w}{B}\frac{dw}{dz}\right)^{f_i}. \tag{12}$$

See the appendix for the derivations. Since dw/dz is not available in the aircraft observations, here the LES results are used to find the relationship among the four dimensionless variables by performing the multivariate polynomial regression. If the power of the right-hand side of Eq. (12) is set to 1,

$$\lambda = \frac{B}{w^2}\left(98.5 - 219.3\frac{\varepsilon}{Bw} + 98.4\frac{w^2}{Br} + 36.0\frac{w}{B}\frac{dw}{dz}\right) \quad (\text{Adjusted } R^2 = 0.42;\ p < 0.01). \tag{13}$$

If the power of the right-hand side of Eq. (12) is set to 2,

$$\lambda = \frac{B}{w^2}\left[69.1 - 237.3\frac{\varepsilon}{Bw}\frac{w^2}{Br} - 224.3\left(\frac{\varepsilon}{Bw}\right)^2 - 18.0\left(\frac{w^2}{Br}\right)^2 + 10.6\left(\frac{w}{B}\frac{dw}{dz}\right)^2 + 49.2\frac{w}{B}\frac{dw}{dz} + 147.8\frac{w^2}{Br} + 2.4\frac{w^2}{Br}\frac{w}{B}\frac{dw}{dz} - 107.5\frac{\varepsilon}{Bw} - 162.2\frac{\varepsilon}{Bw}\frac{w}{B}\frac{dw}{dz}\right] \quad (\text{Adjusted } R^2 = 0.45;\ p < 0.01). \tag{14}$$

If the power of the right-hand side of Eq. (12) is set to 3 and 4, the adjusted R^2 is 0.49 and 0.53, respectively. To compare the results from the Buckingham–Pi analysis and the principal component regression, the relationship between λ with w, B, ε, and r is also obtained using the principal component regression:

$$\lambda = 0.11 w^{-0.17} B^{-0.18} \varepsilon^{-0.19}\left(\frac{1}{r}\right)^{0.081}\left|\frac{1}{w}\frac{dw}{dz}\right|^{0.022} \quad (\text{Adjusted } R^2 = 0.58;\ p < 0.01), \tag{15}$$

where the absolute value of $(1/w)(dw/dz)$ is taken since it could be negative. The addition of r and $(1/w)(dw/dz)$ leads to only a slight increase of the adjusted R^2. Comparison shows that the adjusted R^2 with the Buckingham–Pi theorem increases with the increasing power but is still lower than 0.58 in the principal component regression. More variables, or combinations of variables, with a unit of per meter, may be needed to further improve the fitting. Note that the Buckingham–Pi theorem helps reduce the number of variables from six in Eq. (11) to four in Eq. (12); the dimensionless variables found by using the Buckingham–Pi theorem could be used to elucidate physical mechanisms of entrainment processes.

6. Concluding remarks

Actively growing cumulus clouds sampled in the RACORO field campaign and from the LES using WRF-FASTER are analyzed to develop a new parameterization of λ through examinations of the relationships between λ and w, ε, B, and B/w^2. The results show negative correlations between λ and w, ε, and B, which are attributed to several interacting processes. A larger λ causes lower temperature in the clouds, thus leading to a smaller B. A larger λ causes a smaller w because w is directly driven by B and form drag is created during the entrainment–mixing processes. A smaller w reduces the horizontal shear of w, which is important for turbulence intensity, thus causing a smaller ε. Furthermore, a smaller w means a cloud needs more time to rise a certain height, so the time for the interaction between the cloud and environment is longer and λ is larger (Neggers et al. 2002). Because of the negative correlation between λ and w and the positive correlations between w, ε, and B, λ is negatively correlated with ε and B and positively correlated with B/w^2.

To consider the contributions from all the variables, a parameterization of λ related to w, B, and ε is developed using the approach of principal component regression. This new parameterization, three commonly used parameterizations, and single-variable fitting equations are compared against the directly calculated entrainment rate using observations/simulations. The parameterizations by Neggers et al. (2002), Gregory (2001), and Lin (1999) target for domain mean properties. Here they are applied to individual clouds to test if they can also be used for individual clouds. It is found that the constants assumed in the parameterizations of Neggers et al. (2002) and Gregory (2001) have wide ranges on the individual cloud scale. The fitting result from the observations/simulations show that the exponent in Lin's (1999) parameterization is larger than that reported in Lin (1999). The new parameterization using multiple variables can better represent the directly calculated entrainment rate than the single-variable fitting equations.

The observed and simulated clouds exhibit similar relationships among λ, w, B, and ε, which supports the approach and thus obtains entrainment rate parameterizations even for observations with potential measurement errors, and also suggests that WRF-FASTER can reasonably well reproduce the key entrainment-related quantities and their relationships. The relationships of λ with w, B, and ε from individual cloud samples

and cloud ensembles are similar. The relationships are still valid after considering the effects of the humid shells. In addition, the Buckingham–Pi theorem is used to find the relationships of entrainment rate to related variables and the fitting results are compared with those from the principal component regression.

Some caveats should be pointed out here. First, aliasing problems in aircraft observations may affect the result, as discussed by Lu et al. (2012b,c). It is well known that the turbulence-driven entrainment–mixing process is a highly variable phenomenon and the turbulent eddies range from the macroscopic cloud size down to the Kolmogorov microscopic scale (Gerber et al. 2008); however, most aircraft measurements or LES do not resolve the eddies smaller than the sampling resolution (e.g., ~5 m in observations and 75 m in the LES in this study). Analysis of higher-resolution observations (Lehmann et al. 2009) and simulations (Kumar et al. 2013, 2014) may be needed to address this issue.

Second, the results in this study are based on individual cloud penetrations and, thus, may not be ready for application to cumulus parameterizations representing cumulus ensemble within a grid box of large-scale models; however, the similar intervariable relationships for the cloud ensembles in the LES suggest that the fundamental concepts of this study are applicable even to the cumulus ensembles. The results are a starting point for going from the actual turbulence-scale process to developing a entrainment-rate parameterization for better representing shallow cumulus clouds in the models with the resolutions that do not resolve the shallow cumulus clouds such as analyzed in this study. The results could be a basis for improving shallow clouds that could occur on the grids of deep-convection-permitting models with resolutions of 1–3 km.

Third, error analyses on the variables in the fitting equations are important for aircraft observations. Unfortunately, exact analyses cannot be performed because the measurement errors of vertical velocity, true airspeed, attack angle, and side slip angle are not available. Although the fact that the large-eddy simulation, which does not suffer from observational errors, exhibits similar results as observations suggests that the observational errors are not likely to ruin the fundamental relationships, observational errors may influence regression relationships to some extent, and improving these essential measurements are needed. Examining clouds formed in different environments such as tropical and subtropical oceans is also needed.

Acknowledgments. This research was supported by the National Natural Science Foundation of China (91537108, 91337215, 41305120); China Meteorological Administration Special Public Welfare Research Fund (GYHY201406007, GYHY201406001); the Natural Science Foundation of Jiangsu Province, China (BK20130988); the Specialized Research Fund for the Doctoral Program of Higher Education (20133228120002); the Natural Science Foundation of the Higher Education Institutions of Jiangsu Province, China (13KJB170014); the Open Funding from State Key Laboratory of Numerical Modeling for Atmospheric Sciences and Geophysical Fluid Dynamics; the Open Funding from Key Laboratory of Meteorological Disaster of Ministry of Education, China (KLME1305); the Qing-Lan Project; a Project Funded by the Priority Academic Program Development of Jiangsu Higher Education Institutions; and the U.S. Department of Energy's Atmospheric System Research program and Earth System Modeling program via the FASTER project. Data are from the U.S. Department of Energy's RACORO Campaign (http://www.arm.gov/).

APPENDIX

Derivations Based on the Buckingham–Pi Theorem

In section 5, the Buckingham–Pi theorem is used to find the relationships of entrainment rate λ to related variables. The Buckingham–Pi theorem states that if there is a physically meaningful equation involving n physical variables, then the original equation can be rewritten in terms of a set of $n - k$ dimensionless parameters constructed from the original variables. Here k is the number of physical dimensions involved. In our case, there are two dimensions, L and t, so k is equal to 2; we use two quantities (B and w) to nondimensionalize other quantities:

$$\lambda = \sum_i a_i B^{b_{1i}+b_{2i}+b_{3i}} w^{c_{1i}+c_{2i}+c_{3i}} \varepsilon^{d_i} \left(\frac{1}{r}\right)^{e_i} \left(\frac{1}{w}\frac{dw}{dz}\right)^{f_i}$$
$$= \sum_i a_i [B^{b_{1i}} w^{c_{1i}} \varepsilon^{d_i}] \left[B^{b_{2i}} w^{c_{2i}} \left(\frac{1}{r}\right)^{e_i}\right] \left[B^{b_{3i}} w^{c_{3i}} \left(\frac{1}{w}\frac{dw}{dz}\right)^{f_i}\right], \quad \text{(A1)}$$

where a_i, b_{1i}, b_{2i}, b_{3i}, c_{1i}, c_{2i}, c_{3i}, d_i, e_i, and f_i are parameters; B, w, ε, r, and z are buoyancy, vertical velocity, dissipation rate, cloud radius, and height, respectively. In Eq. (A1), λ is written as the sum of i terms including w, B, ε, r, and $(1/w)(dw/dz)$, where $i = 1, 2, 3, \ldots$, and the maximum i depends on the power of Eq. (11). One of the three quantities, $B^{b_{1i}} w^{c_{1i}} \varepsilon^{d_i}$, $B^{b_{2i}} w^{c_{2i}} (1/r)^{e_i}$, and $B^{b_{3i}} w^{c_{3i}} [(1/w)(dw/dz)]^{f_i}$ must have the same unit as λ and

the rest have the unit of one to keep the units at the left- and right-hand sides of Eq. (A1) equal. If $B^{b_{1i}}w^{c_{1i}}\varepsilon^{d_i}$ is set to have the same unit as λ, then

$$\mathrm{m}^{-1} = (\mathrm{m\,s}^{-2})^{b_{1i}}(\mathrm{m\,s}^{-1})^{c_{1i}}(\mathrm{m}^2\,\mathrm{s}^{-3})^{d_i}. \tag{A2}$$

Equating the units on both sides of the equation requires that

$$b_{1i} = 1 - d_i \quad \text{and} \tag{A3a}$$
$$c_{1i} = -2 - d_i. \tag{A3b}$$

Therefore,

$$B^{b_{1i}}w^{c_{1i}}\varepsilon^{d_i} = (\varepsilon/Bw)^{d_i}(B/w^2). \tag{A4}$$

Setting the unit of $B^{b_{2i}}w^{c_{2i}}(1/r)^{e_i}$ to one leads to

$$(\mathrm{m\,s}^{-2})^{b_{2i}}(\mathrm{m\,s}^{-1})^{c_{2i}}(\mathrm{m}^{-1})^{e_i} = 1. \tag{A5}$$

This gives

$$b_{2i} = -e_i, \tag{A6a}$$
$$c_{2i} = 2e_i, \tag{A6b}$$

and

$$B^{b_{2i}}w^{c_{2i}}(1/r)^{e_i} = (w^2/Br)^{e_i}. \tag{A7}$$

Setting the unit of $B^{b_{3i}}w^{c_{3i}}[(1/w)(dw/dz)]^{f_i}$ to one leads to

$$(\mathrm{m\,s}^{-2})^{b_{3i}}(\mathrm{m\,s}^{-1})^{c_{3i}}(\mathrm{m}^{-1})^{f_i} = 1. \tag{A8}$$

Thus,

$$b_{3i} = -f_i, \tag{A9a}$$
$$c_{3i} = 2f_i, \tag{A9b}$$

and

$$B^{b_{3i}}w^{c_{3i}}\left(\frac{1}{w}\frac{dw}{dz}\right)^{f_i} = \left(\frac{w}{B}\frac{dw}{dz}\right)^{f_i}. \tag{A10}$$

Using Eqs. (A4), (A7), and (A10), Eq. (A1) becomes

$$\frac{\lambda}{B/w^2} = \sum_i a_i\left(\frac{\varepsilon}{Bw}\right)^{d_i}\left(\frac{w^2}{Br}\right)^{e_i}\left(\frac{w}{B}\frac{dw}{dz}\right)^{f_i}. \tag{A11}$$

The results are the same if $B^{b_{2i}}w^{c_{2i}}(1/r)^{e_i}$ or $B^{b_{3i}}w^{c_{3i}}[(1/w)(dw/dz)]^{f_i}$ are set to have the same unit as λ.

REFERENCES

Arakawa, A., and W. H. Schubert, 1974: Interaction of a cumulus cloud ensemble with the large-scale environment, part I. *J. Atmos. Sci.*, **31**, 674–701, doi:10.1175/1520-0469(1974)031<0674:IOACCE>2.0.CO;2.

Bajpai, N., 2009: *Business Statistics*. Pearson, 794 pp.

Betts, A. K., 1975: Parametric interpretation of trade-wind cumulus budget studies. *J. Atmos. Sci.*, **32**, 1934–1945, doi:10.1175/1520-0469(1975)032<1934:PIOTWC>2.0.CO;2.

Blossey, P. N., and Coauthors, 2013: Marine low cloud sensitivity to an idealized climate change: The CGILS LES intercomparison. *J. Adv. Model. Earth Syst.*, **5**, 234–258, doi:10.1002/jame.20025.

Blyth, A. M., 1993: Entrainment in cumulus clouds. *J. Appl. Meteor.*, **32**, 626–641, doi:10.1175/1520-0450(1993)032<0626:EICC>2.0.CO;2.

Cai, Q., G. J. Zhang, and T. Zhou, 2013: Impacts of shallow convection on MJO simulation: A moist static energy and moisture budget analysis. *J. Climate*, **26**, 2417–2431, doi:10.1175/JCLI-D-12-00127.1.

Chan, K. R., J. Dean-Day, S. W. Bowen, and T. P. Bui, 1998: Turbulence measurements by the DC-8 Meteorological Measurement System. *Geophys. Res. Lett.*, **25**, 1355–1358, doi:10.1029/97GL03590.

Dawe, J. T., and P. H. Austin, 2013: Direct entrainment and detrainment rate distributions of individual shallow cumulus clouds in an LES. *Atmos. Chem. Phys.*, **13**, 7795–7811, doi:10.5194/acp-13-7795-2013.

Deardorff, J., 1980: Stratocumulus-capped mixed layers derived from a three-dimensional model. *Bound.-Layer Meteor.*, **18**, 495–527, doi:10.1007/BF00119502.

Del Genio, A. D., and J. Wu, 2010: The role of entrainment in the diurnal cycle of continental convection. *J. Climate*, **23**, 2722–2738, doi:10.1175/2009JCLI3340.1.

Deng, Z., C. Zhao, Q. Zhang, M. Huang, and X. Ma, 2009: Statistical analysis of microphysical properties and the parameterization of effective radius of warm clouds in Beijing area. *Atmos. Res.*, **93**, 888–896, doi:10.1016/j.atmosres.2009.04.011.

de Rooy, W. C., and A. P. Siebesma, 2010: Analytical expressions for entrainment and detrainment in cumulus convection. *Quart. J. Roy. Meteor. Soc.*, **136**, 1216–1227.

Diskin, G. S., J. R. Podolske, G. W. Sachse, and T. A. Slate, 2002: Open-path airborne tunable diode laser hygrometer. *Diode Lasers and Applications in Atmospheric Sensing*, A. Fried, Ed., International Society for Optical Engineering (SPIE Proceedings, Vol. 4817), 196–204, doi:10.1117/12.453736.

Endo, S., and Coauthors, 2015: RACORO continental boundary layer cloud investigations: 2. Large-eddy simulations of cumulus clouds and evaluation with in situ and ground-based observations. *J. Geophys. Res. Atmos.*, **120**, 5993–6014, doi:10.1002/2014JD022525.

Gerber, H. E., G. M. Frick, J. B. Jensen, and J. G. Hudson, 2008: Entrainment, mixing, and microphysics in trade-wind cumulus. *J. Meteor. Soc. Japan*, **86A**, 87–106, doi:10.2151/jmsj.86A.87.

Grant, A. L. M., and A. R. Brown, 1999: A similarity hypothesis for shallow cumulus transports. *Quart. J. Roy. Meteor. Soc.*, **125**, 1913–1936, doi:10.1002/qj.49712555802.

Gregory, D., 2001: Estimation of entrainment rate in simple models of convective clouds. *Quart. J. Roy. Meteor. Soc.*, **127**, 53–72, doi:10.1002/qj.49712757104.

Heus, T., and H. J. J. Jonker, 2008: Subsiding shells around shallow cumulus clouds. *J. Atmos. Sci.*, **65**, 1003–1018, doi:10.1175/2007JAS2322.1.

Jolliffe, I. T., 1982: A note on the use of principal components in regression. *J. Roy. Stat. Soc.*, **31C**, 300–303, doi:10.2307/2348005.

Kumar, B., J. Schumacher, and R. Shaw, 2013: Cloud microphysical effects of turbulent mixing and entrainment. *Theor. Comput. Fluid Dyn.*, **27**, 361–376, doi:10.1007/s00162-012-0272-z.

——, ——, and ——, 2014: Lagrangian mixing dynamics at the cloudy–clear air interface. *J. Atmos. Sci.*, **71**, 2564–2580, doi:10.1175/JAS-D-13-0294.1.

Lawson, R. P., and W. A. Cooper, 1990: Performance of some airborne thermometers in clouds. *J. Atmos. Oceanic Technol.*, **7**, 480–494, doi:10.1175/1520-0426(1990)007<0480:POSATI>2.0.CO;2.

Lehmann, K., H. Siebert, and R. A. Shaw, 2009: Homogeneous and inhomogeneous mixing in cumulus clouds: Dependence on local turbulence structure. *J. Atmos. Sci.*, **66**, 3641–3659, doi:10.1175/2009JAS3012.1.

Lin, C., 1999: Some bulk properties of cumulus ensembles simulated by a cloud-resolving model. Part II: Entrainment profiles. *J. Atmos. Sci.*, **56**, 3736–3748, doi:10.1175/1520-0469(1999)056<3736:SBPOCE>2.0.CO;2.

Lin, W., and Coauthors, 2015: RACORO continental boundary layer cloud investigations: 3. Separation of parameterization biases in single-column model CAM5 simulations of shallow cumulus. *J. Geophys. Res. Atmos.*, **120**, 6015–6033, doi:10.1002/2014JD022524.

Lu, C., Y. Liu, S. Niu, and A. M. Vogelmann, 2012a: Observed impacts of vertical velocity on cloud microphysics and implications for aerosol indirect effects. *Geophys. Res. Lett.*, **39**, L21808, doi:10.1029/2012GL053599.

——, ——, ——, and ——, 2012b: Lateral entrainment rate in shallow cumuli: Dependence on dry air sources and probability density functions. *Geophys. Res. Lett.*, **39**, L20812, doi:10.1029/2012GL053646.

——, ——, S. S. Yum, S. Niu, and S. Endo, 2012c: A new approach for estimating entrainment rate in cumulus clouds. *Geophys. Res. Lett.*, **39**, L04802, doi:10.1029/2011GL050546.

——, S. Niu, Y. Liu, and S. Niu, 2013: Empirical relationship between entrainment rate and microphysics in cumulus clouds. *Geophys. Res. Lett.*, **40**, 2333–2338, doi:10.1002/grl.50445.

——, Y. Liu, and S. Niu, 2014a: Entrainment-mixing parameterization in shallow cumuli and effects of secondary mixing events. *Chin. Sci. Bull.*, **59**, 896–903, doi:10.1007/s11434-013-0097-1.

——, ——, ——, and S. Endo, 2014b: Scale dependence of entrainment-mixing mechanisms in cumulus clouds. *J. Geophys. Res. Atmos.*, **119**, 13 877–13 890, doi:10.1002/2014JD022265.

Mlawer, E. J., S. J. Taubman, P. D. Brown, M. J. Iacono, and S. A. Clough, 1997: Radiative transfer for inhomogeneous atmospheres: RRTM, a validated correlated-k model for the longwave. *J. Geophys. Res.*, **102**, 16 663–16 682, doi:10.1029/97JD00237.

Morrison, H., J. A. Curry, and V. I. Khvorostyanov, 2005: A new double-moment microphysics parameterization for application in cloud and climate models. Part I: Description. *J. Atmos. Sci.*, **62**, 1665–1677, doi:10.1175/JAS3446.1.

Neggers, R. A. J., A. P. Siebesma, and H. J. J. Jonker, 2002: A multiparcel model for shallow cumulus convection. *J. Atmos. Sci.*, **59**, 1655–1668, doi:10.1175/1520-0469(2002)059<1655:AMMFSC>2.0.CO;2.

Podolske, J. R., G. W. Sachse, and G. S. Diskin, 2003: Calibration and data retrieval algorithms for the NASA Langley/Ames Diode Laser Hygrometer for the NASA Transport and Chemical Evolution Over the Pacific (TRACE-P) mission. *J. Geophys. Res.*, **108**, 8792, doi:10.1029/2002JD003156.

Romps, D. M., 2010: A direct measure of entrainment. *J. Atmos. Sci.*, **67**, 1908–1927, doi:10.1175/2010JAS3371.1.

Schmid, B., and Coauthors, 2014: The DOE ARM Aerial Facility. *Bull. Amer. Meteor. Soc.*, **95**, 723–742, doi:10.1175/BAMS-D-13-00040.1.

Simpson, J., 1971: On cumulus entrainment and one-dimensional models. *J. Atmos. Sci.*, **28**, 449–455, doi:10.1175/1520-0469(1971)028<0449:OCEAOD>2.0.CO;2.

Squires, P., and J. S. Turner, 1962: An entraining jet model for cumulo-nimbus updraughts. *Tellus*, **14A**, 422–434, doi:10.1111/j.2153-3490.1962.tb01355.x.

Turner, J. S., 1962: The ''starting plume'' in neutral surroundings. *J. Fluid Mech.*, **13**, 356–368, doi:10.1017/S0022112062000762.

Vogelmann, A. M., and Coauthors, 2012: RACORO extended-term aircraft observations of boundary layer clouds. *Bull. Amer. Meteor. Soc.*, **93**, 861–878, doi:10.1175/BAMS-D-11-00189.1.

——, and Coauthors, 2015: RACORO continental boundary layer cloud investigations: 1. Case study development and ensemble large-scale forcings. *J. Geophys. Res. Atmos.*, **120**, 5962–5992, doi:10.1002/2014JD022713.

von Salzen, K., and N. A. McFarlane, 2002: Parameterization of the bulk effects of lateral and cloud-top entrainment in transient shallow cumulus clouds. *J. Atmos. Sci.*, **59**, 1405–1430, doi:10.1175/1520-0469(2002)059<1405:POTBEO>2.0.CO;2.

Wang, X., and M. Zhang, 2014: Vertical velocity in shallow convection for different plume types. *J. Adv. Model. Earth Syst.*, **6**, 478–489, doi:10.1002/2014MS000318.

——, Q. Bao, K. Liu, G. Wu, and Y. Liu, 2011: Features of rainfall and latent heating structure simulated by two convective parameterization schemes. *Sci. China Earth Sci.*, **54**, 1779–1788, doi:10.1007/s11430-011-4282-2.

Wang, Y., L. Zhou, and K. Hamilton, 2007: Effect of convective entrainment/detrainment on the simulation of the tropical precipitation diurnal cycle. *Mon. Wea. Rev.*, **135**, 567–585, doi:10.1175/MWR3308.1.

Wu, X., L. Deng, X. Song, G. Vettoretti, W. R. Peltier, and G. J. Zhang, 2007: Impact of a modified convective scheme on the Madden-Julian Oscillation and El Niño–Southern Oscillation in a coupled climate model. *Geophys. Res. Lett.*, **34**, L16823, doi:10.1029/2007GL030637.

Xie, S., R. T. Cederwall, and M. Zhang, 2004: Developing long-term single-column model/cloud system–resolving model forcing data using numerical weather prediction products constrained by surface and top of the atmosphere observations. *J. Geophys. Res.*, **109**, D01104, doi:10.1029/2003JD004045.

Zhang, G. J., and X. Song, 2009: Interaction of deep and shallow convection is key to Madden-Julian Oscillation simulation. *Geophys. Res. Lett.*, **36**, L09708, doi:10.1029/2009GL037340.

Zhang, M. H., J. L. Lin, R. T. Cederwall, J. J. Yio, and S. C. Xie, 2001: Objective analysis of ARM IOP data: Method and sensitivity. *Mon. Wea. Rev.*, **129**, 295–311, doi:10.1175/1520-0493(2001)129<0295:OAOAID>2.0.CO;2.